Journal of the Optical Society of America A
OPTICS, IMAGE SCIENCE, AND VISION

Nonuniformity correction for an infrared focal plane array based on diamond search block matching

RONG SHENG-HUI,[1] ZHOU HUI-XIN,[1,*] QIN HAN-LIN,[1] LAI RUI,[2] AND QIAN KUN[1]

[1]School of Physics and Optoelectronic Engineering, Xidian University, Xi'an, Shaanxi 710071, China
[2]School of Microelectronics, Xidian University, Xi'an, Shaanxi 710071, China
*Corresponding author: hxzhou@mail.xidian.edu.cn

Received 29 December 2015; revised 19 March 2016; accepted 30 March 2016; posted 1 April 2016 (Doc. ID 256562); published 20 April 2016

In scene-based nonuniformity correction algorithms, artificial ghosting and image blurring degrade the correction quality severely. In this paper, an improved algorithm based on the diamond search block matching algorithm and the adaptive learning rate is proposed. First, accurate transform pairs between two adjacent frames are estimated by the diamond search block matching algorithm. Then, based on the error between the corresponding transform pairs, the gradient descent algorithm is applied to update correction parameters. During the process of gradient descent, the local standard deviation and a threshold are utilized to control the learning rate to avoid the accumulation of matching error. Finally, the nonuniformity correction would be realized by a linear model with updated correction parameters. The performance of the proposed algorithm is thoroughly studied with four real infrared image sequences. Experimental results indicate that the proposed algorithm can reduce the nonuniformity with less ghosting artifacts in moving areas and can also overcome the problem of image blurring in static areas.

OCIS codes: (110.3080) Infrared imaging; (100.2550) Focal-plane-array image processors; (040.3060) Infrared; (110.4280) Noise in imaging systems; (100.3020) Image reconstruction-restoration.

http://dx.doi.org/10.1364/JOSAA.33.000938

1. INTRODUCTION

Due to the immature manufacturing process, fixed pattern noise (FPN) caused by nonuniformity seriously degrades the sensitivity and quality of the infrared focal plane array (IRFPA) imaging system [1]. It is essential to develop effective nonuniformity correction (NUC) algorithms to achieve high-quality infrared images.

NUC algorithms mainly contain the reference-based nonuniformity correction (RBNUC) algorithm and the scene-based nonuniformity correction (SBNUC) algorithm. The RBNUC algorithm employs a uniform blackbody as the reference irradiance source to calculate the correction parameter [2,3]. Its advantages lie in its simplicity and low computational complexity. However, repeating the correction process is needed due to the temporal drift of the detector's response characteristics. Compared with RBNUC, SBNUC algorithms only rely on the information of the imaging scene, which would reduce the operation complexity and avoid imaging interruption.

Over the years, four typical SBNUC algorithms have been researched deeply. (1) The constant-statistics-based NUC (CS-NUC) algorithm [4]. This algorithm assumes that the first- and second-order statistics of each detector's output should be the same over a sufficient number of frames. (2) The temporal-high-pass-filtering-based NUC (THP-NUC) algorithm [5]. This algorithm sets a high-pass filter in the temporal domain, and the FPN will be removed due to its low-frequency characteristics. (3) The least-mean-square-error-based NUC (LMS-NUC) algorithm [6]. This algorithm uses a least mean square algorithm to adaptively determine the nonuniformity model parameter to achieve good correction performance. (4) The registration-based NUC (RG-NUC) algorithm [7]. This algorithm corrects the FPN under the assumption that different detectors between two adjacent frames should have identical response when observing the same scene.

However, most of the SBNUC algorithms suffer from the drawback of artificial ghosting and image blurring. Generally, when a portion of scene in the image temporarily slows or halts, image blurring would occur, because these correction algorithms cannot distinguish the static object and the unchanging FPN. After the scene motion resumes, ghosting would occur in the reserve direction of the motion, because the correction parameter cannot update as fast as the scene changes.

Many improved algorithms have been proposed in recent years. For CS algorithms, a motion detection gate was proposed

in [8] to deal with burn-in ghosting. For THP algorithms, a spatial low-pass filter is utilized to separate the raw image in [9], and only the spatial high-pass part of the image is utilized to estimate the FPN. For LMS algorithms, the desired image [10–12] and the adaptive learning rate [13] are the two key factors to improve the performance of NUC.

Compared with other SBNUC algorithms, the results of RG-NUC have less ghosting and image blurring [14–16]. In the ideal registration situation, these algorithms can be highly effective. Fewer frames are required for convergence of correction parameters. Besides, only two adjacent frames rather than the statistical data of all the previous frames will be analyzed. Therefore, correction results have less artificial ghosting and image blurring.

Nevertheless, sometimes scenes in an image do not share the same motion vector. Local motion and distortion between consecutive frames would lead to this algorithm being inapplicable.

Considering the drawback of the traditional RG-NUC, in this paper, an improved algorithm is proposed based on a diamond search block matching algorithm and an adaptive learning rate. A group of local motive vectors obtained by the diamond search (DS) algorithm can effectively reflect changes of a scene compared with one global motion vector. Furthermore, an adaptive learning rate based on the local standard deviation and a threshold are utilized to decline the matching error further.

The remainder of the paper is organized as follows. In Section 2, the response and correction model of the detector are given first, and then the main idea of RG-NUC is discussed in detail. In Section 3, an improved correction algorithm based on the diamond search block matching algorithm is proposed. In Section 4, an adaptive learning rate is introduced to decline the matching error further. In Section 5, the performance of the proposed algorithm is verified with two infrared image sequences, and the conclusion is given in Section 6.

2. REGISTRATION-BASED NONUNIFORMITY CORRECTION

A. Response and Correction Model

The response of each detector in an IRFPA can be approximated as a linear model defined as

$$x_{i,j}^n = a_{i,j}^n \cdot y_{i,j}^n + b_{i,j}^n, \tag{1}$$

where n is the frame number, i and j indicate the detector location, $x_{i,j}^n$ is the detector response, $y_{i,j}^n$ is the real infrared radiation exposed on this detector, and $a_{i,j}^n$ and $b_{i,j}^n$ are linear model parameters.

NUC algorithms aim to find the real infrared radiation $y_{i,j}^n$ by estimating the correction coefficients with the readout value $x_{i,j}^n$, which could be expressed as

$$\hat{y}_{i,j}^n = G_{i,j}^n \cdot x_{i,j}^n + O_{i,j}^n, \tag{2}$$

where $\hat{y}_{i,j}^n$ is the corrected output, and $G_{i,j}^n = 1/a_{i,j}^n$ and $O_{i,j}^n = -b_{i,j}^n/a_{i,j}^n$ are the NUC gain and offset correction parameters, respectively. If ideal correction parameters $G_{i,j}^n$ and $O_{i,j}^n$ were obtained, the process of NUC could be realized by Eq. (2).

B. Registration-Based Nonuniformity Correction

The RG-NUC algorithm assumes that different detectors exposed to the same scene should output the same value, which could be expressed in Fig. 1. As can be seen in this figure, an object is located at (u, v) in frame n-1 initially, and then it moves to (i, j) in frame n. Supposing the infrared radiation of the object between two adjacent frames is identical, the gray value in the image will be invariant. For instance, the gray value of the object center is 45 in both image frames.

This assumption can be defined as

$$y_{i,j}^n - y_{u,v}^{n-1} = 0, \tag{3}$$

where n is the frame number, and the coordinates (i, j) and (u, v) are two corresponding detector coordinates exposed by the same scene. These coordinates, such as (i, j) and (u, v), are called a transform pair in this paper. Obviously, changes in radiation, scale, and projection between the two adjacent frames are ignored.

In fact, though exposed by the same scene, different detectors output differently due to response nonuniformity, and Eq. (3) is not valid. In the RG-NUC algorithm, an error function at the coordinates (i, j) is defined as Eq. (3) to describe this output difference as

$$e_{i,j}^n = \hat{y}_{i,j}^n - \hat{y}_{u,v}^{n-1}, \tag{4}$$

where (i, j) and (u, v) are a transform pair, and $\hat{y}_{i,j}^n$ and $\hat{y}_{u,v}^{n-1}$ are corrected outputs in the frame n and frame $(n$-$1)$, respectively, which are expressed as

$$\hat{y}_{i,j}^n = G_{i,j}^n \cdot x_{i,j}^n + O_{i,j}^n, \tag{5}$$

$$\hat{y}_{u,v}^{n-1} = G_{u,v}^n \cdot x_{u,v}^{n-1} + O_{u,v}^n. \tag{6}$$

By this means, the first step of RG-NUC is to determine the transform pair (i, j) and (u, v) between two adjacent frames. The next step is to find a proper way to adjust the correction parameters frame by frame to minimize the error function $e_{i,j}^n$.

The traditional registration-based correction algorithm exploits the global motion between two adjacent frames to extract information about the FPN. It is highly effective in the translational transform situation because all the pixels in an image have the same motion vector between two adjacent frames. Accurate transform pairs could be achieved by one global motion vector.

However, if there were some complex motions, such as local motion, one global motion vector could not accurately reflect the motion status of all the pixels in an image. Inaccurate transform pairs would result in serious degradation of correction performance, which is very common in practice.

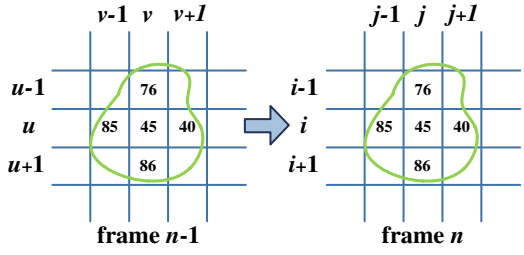

Fig. 1. Presentation of RG-NUC.

3. DS-BLOCK-MATCHING-BASED NUC

As mentioned above, the drawback of the traditional RG-NUC is mainly caused by the inaccurate transform pairs and the global motion vector cannot describe the motion trend accurately, especially scenes with local motion.

In order to achieve higher correction performance, a viable solution is to utilize a group of motion vectors to describe changes between two adjacent frames, rather than one global motion vector. For instance, the moving part and the static part of scene are described by different motion vectors. The correction error caused by the only global motion vector can be eliminated.

In order to achieve a group of motion vectors to improve the correction performance, the diamond search block matching algorithm is applied in this paper.

A. Diamond Search Block Matching Algorithm

The DS block matching algorithm is an outstanding motion estimation algorithm, which is widely utilized in video compression applications [17]. First, the current frame is divided into a matrix of macro blocks. Then, each macro block is compared with its adjacent neighbors in the previous frame. The least mean absolute difference (MAD) is utilized to measure the matching of one macro block with another, which is defined as

$$\mathrm{MAD} = \frac{1}{N^2}\sum_{i=0}^{N-1}\sum_{j=0}^{N-1}|C_{ij} - R_{ij}|, \tag{7}$$

where N is the size of the macro block, and C_{ij} and R_{ij} are the pixels being compared in the current macro block and the reference macro block, respectively.

The macro block that results in the least MAD is the one that matches the closest to the current block. The final search point in this macro block is called the minimum block distortion (MDB) point. Then, the motion vector and the transform pairs can be calculated by pointing the matched block in the previous frame to the corresponding block in current frame.

In order to boost the search speed, a large diamond search pattern (LDSP) and a small diamond search pattern (SDSP) are utilized. The LDSP selects nine checking points, as shown in Fig. 2(a), and the SDSP selects five checking points, as shown in Fig. 2(b).

The detailed steps of the DS block matching algorithm are summarized as follows.

Step 1: The initial LDSP is centered at the origin of the search window, the MADs of nine checking points are calculated successively, and then the MDB point is identified. If the MDB point is just located at the center point of the LDSP, which is the origin of the search window, then go to Step 3; otherwise, go to Step 2.

Step 2: The MBD point found in the previous search step is repositioned as the center point of a new LDSP to identify a new MBD point. If the new MBD point obtained in this step is located at the center position of the new LDSP, then go to Step 3; otherwise, recursively repeat this step.

Step 3: Switch the search pattern from a LDSP to a SDSP. MAD of the five checking points in the SDSP are calculated successively to identify the MDB point. The MBD point found in this step is the final solution of the motion vector, which points to the best matching block.

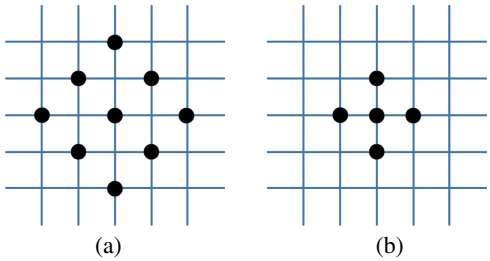

Fig. 2. Search patterns. (a) LDSP and (b) SDSP.

In order to illustrate the effectiveness of the DS block matching algorithm, an experiment is implemented, and the results are shown in Fig. 3. Two adjacent frames selected from an infrared sequence are tested by the DS block matching algorithm. As can be seen in Fig. 3(a), a girl is moving from the right to the left. Thus, the difference image has significant fluctuations.

A group of motion vectors can be calculated by the DS algorithm shown in Fig. 3(b). These vectors have different directions and sizes which can accurately reflect the changes between the two adjacent frames.

Based on the motion vectors, a compensated image can be achieved, and the difference image between the compensated image and the nth frame is shown in Fig. 3(c). Only a few unmatched points can be seen. Thus, the DS block matching algorithm can reflect the motion between two adjacent frames and achieve the transform pair accurately.

As the search pattern is neither too small nor too big and the fact that there is no limit to the number of steps, the DS algorithm can ensure the accuracy of matching and improve the search speed [18]. Therefore, by means of the DS algorithm, the map of transform pairs between two adjacent frames can be obtained accurately and quickly.

B. DS-Block-Matching-Based NUC

In the RG-NUC algorithm, after achieving transform pairs, the next step is to adjust the correction parameters to minimize the error function $e_{i,j}^n$ in Eq. (4) and in the proposed algorithm, an iterative process is applied as follows.

In order to simplify, we take the pixel (i, j) into the consideration. First, a cost function is defined as

$$F_{i,j}^n = (e_{i,j}^n)^2 = (\hat{y}_{i,j}^n - \hat{y}_{u,v}^{n-1})^2 = (G_{i,j}^n \cdot x_{i,j}^n + O_{i,j}^n - \hat{y}_{u,v}^{n-1})^2. \tag{8}$$

Then, the next task is to minimize the cost function F. Here, the steepest descent algorithm is applied in which the iteration direction is given by the derivative of F to G and O at the coordinates (i, j):

$$\frac{\partial F_{i,j}^n}{\partial G_{i,j}^n} = 2x_{i,j}^n \cdot (G_{i,j}^n \cdot x_{i,j}^n + O_{i,j}^n - \hat{y}_{u,v}^{n-1}) = 2 \cdot x_{i,j}^n \cdot e_{i,j}^n, \tag{9}$$

$$\frac{\partial F_{i,j}^n}{\partial O_{i,j}^n} = 2(G_{i,j}^n \cdot x_{i,j}^n + O_{i,j}^n - \hat{y}_{u,v}^{n-1}) = 2 \cdot e_{i,j}^n. \tag{10}$$

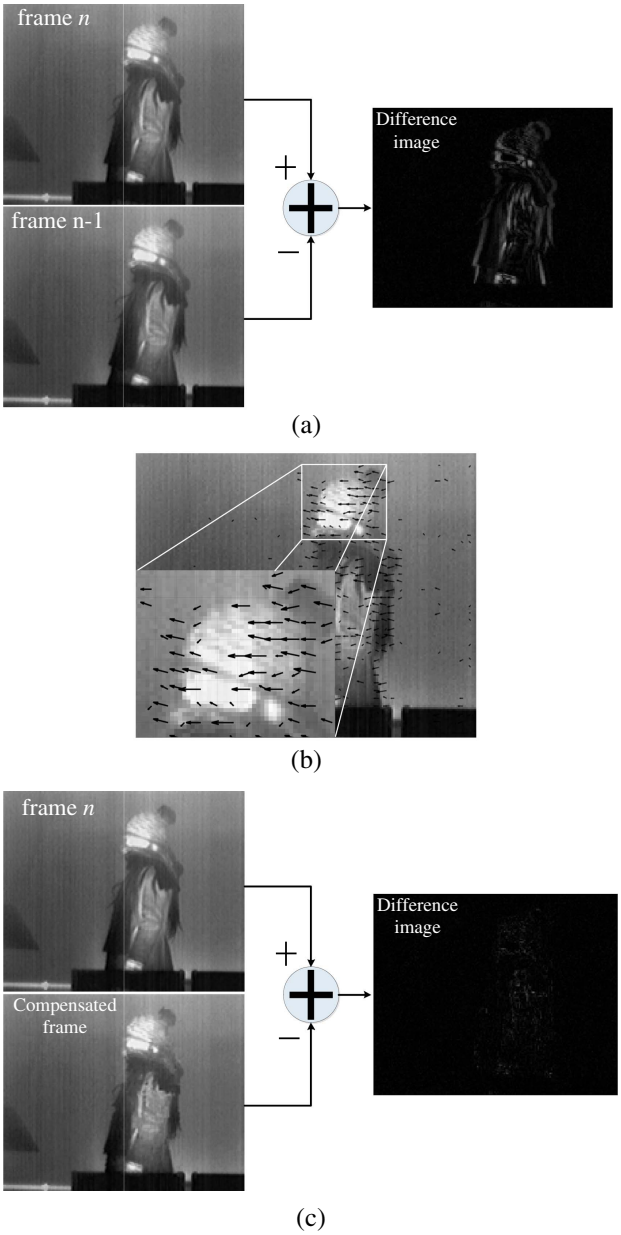

Fig. 3. DS block matching result. (a) Raw-image-based difference image, (b) motion vectors, and (c) DS block matching difference image.

By this means, the NUC parameters are updated recursively with a portion of each respective error gradient, which are indicated as Eqs. (11) and (12), respectively, as follows:

$$G_{i,j}^{n+1} = G_{i,j}^{n} - 2\alpha x_{i,j}^{n} \cdot e_{i,j}^{n}, \tag{11}$$

$$O_{i,j}^{n+1} = O_{i,j}^{n} - 2\alpha e_{i,j}^{n}, \tag{12}$$

where the small positive parameter α called the learning rate controls the convergence step size. Generally, a larger α value can provide a faster convergence speed, while a smaller value can assure better stability instead. The learning rate will be discussed in detail in Section 4.

Finally, the NUC will be realized by Eq. (2) with the updated correction parameters $G_{i,j}^{n}$ and $O_{i,j}^{n}$.

4. IMPROVE DSBM-NUC BY THE ADAPTIVE LEARNING RATE

Due to the change in radiation, scale, and projection between two adjacent frames, inaccurate transform pairs achieved by the DS block matching algorithm are still unavoidable. As can be seen in Fig. 3(d), a few unmatched points still exist. Inaccurate block matching would lead to blocking artifacts [19] and eventually impacts the performance of the correction. Thus, the adaptive learning rate is proposed to decline the matching error further.

A. Adjust the Learning Rate with a Threshold

In an ideal matching situation, the error function $e_{i,j}^{n}$ is only caused by the FPN. Compared with the range of image gray scale, the value of the FPN is relatively smaller. Thus, the value of $e_{i,j}^{n}$ is very small in the matched place. If a large value of $e_{i,j}^{n}$ exists, it was probably caused by inaccurate matching.

Here, a threshold T is introduced to eliminate errors caused by unmatchable parts of the image. If $e_{i,j}^{n}$ is larger than the threshold T in some parts of the image, it is mainly cause by inaccurate matching. Thus, NUC parameters should not be updated, and if $e_{i,j}^{n}$ is less than T, the NUC parameters should be updated.

B. Adjust the Learning Rate with the Local Standard Deviation

However, the threshold strategy is only suitable in places with large image fluctuations, such as sharp edges. In smooth places, image fluctuations are smaller, and no matter whether the image is matched or not, the error function $e_{i,j}^{n}$ has a small value. Thus, in this place, it is difficult to determine if the value of $e_{i,j}^{n}$ is caused by FPN or error matching. Thus, a new metric should be introduced to measure the accuracy of matching in smooth places.

Inspired by [13], the standard deviation acts as a confidence measure of the desired image. In this paper, the standard deviation is introduced as the confidence measure of the matching accuracy in smooth places.

The block matching algorithm matches the optimal point depending on the local information of images. In places with abundant information, such as edges and areas with fine texture, the standard deviation is larger. Besides, there are great differences between MADs of the checking points. FPN has little influence on this area, and it is easy to determine the right MDB point. Thus, it is reasonable to utilize a larger learning rate to increase the convergence speed in this place.

Otherwise, in the smooth place of the image, the standard deviation is smaller. Besides, the MADs of the checking points are similar or equal. It is susceptible to FPN, and the false MDB point may achieved. An inaccurate MDB point means an incorrect update of correction parameters. Therefore, it is reasonable to apply the smaller learning rate in this area to alleviate the error correction.

The local standard deviation has the same tendency with the learning rate. A larger local standard deviation means more

accurate matching, and a smaller learning rate should be selected in the smooth area to avoid updating the inaccurate correction parameter.

As mentioned above, in this paper, each pixel is given an independent adaptive learning rate defined as

$$\alpha_{i,j}^{n} = \begin{cases} k \cdot \delta_{i,j}^{n}, & |e_{i,j}^{n}| < T, \\ 0, & |e_{i,j}^{n}| > T, \end{cases} \tag{13}$$

where n is the frame number, and k is a constant parameter. $\delta_{i,j}^{n}$ is the local standard deviation in the window of 3×3. The threshold T is determined by the FPN degree and can be chosen by trial and error. If the degree of FPN is serious, the value of T will be larger. Otherwise, if the degree of FPN is slight, the value of T will be smaller.

C. DS-Block-Matching-Based NUC with the Adaptive Learning Rate

In summary, the flow chart of the proposed NUC algorithm is shown as Fig. 4, and the detailed steps are summarized as follows (the pixel coordinates are omitted for simplicity).

Step 1: Initialize correction parameters $\boldsymbol{G} = 1$, $\boldsymbol{O} = 0$.
Step 2: Input two adjacent infrared frames x^n and x^{n-1} from the infrared sequence.
Step 3: Execute the correction process by Eqs. (5) and (6) to achieve the corrected output $\hat{y}^n$ and $\hat{y}^{n-1}$.
Step 4: Calculate motion vectors between the corrected output $\hat{y}^n$ and $\hat{y}^{n-1}$ by the DS block matching algorithm.
Step 5: Calculate the motion-compensated image by $\hat{y}^{n-1}$ and motion vectors.
Step 6: Subtract the compensated image form $\hat{y}^n$ to calculate the error function e^n.
Step 7: Update the NUC parameters $\boldsymbol{G}$ and $\boldsymbol{O}$ by Eqs. (11) and (12); the learning rate will be controlled by Eq. (13).
Step 8: Repeat Step 2 to Step 7.

5. EXPERIMENT RESULTS AND ANALYSIS

A. Experiment Description

Four real infrared sequences obtained by an uncooled infrared camera (8–12 μm) are utilized to evaluate the effectiveness of the proposed algorithm. The original images selected from sequences are shown in Fig. 5, where the stripe FPN influences the image quality seriously. Figure 5(a) is the 120th frame of sequence 1, Fig. 5(b) is the 140th frame of sequence 2, and Figs. 5(c) and 5(d) are the 130th frame and 100th frame of sequence 3 and sequence 4, respectively.

The first infrared image sequence was acquired by moving the camera steadily and slowly. Thus, all of the objects in the image share the same motion vector. By this sequence, the performance of the correction algorithm in the simple motion situation can be tested. The second infrared image sequence contains a reciprocating walking girl with a static background. There is a clear static pipeline in left bottom corner of the image. By this experiment with the second sequence, the performance of the correction algorithm in the complex motion situation can be tested. The third and fourth sequences were captured under general conditions, where both local and global motion existed. By this experiment, practicability of algorithms can be tested.

In the proposed algorithm, the search window size is 7, the macro block size is 4, the learning rate k is set as 0.006, and the threshold T is set as 0.1. All images were linearly mapped to the range of 0 to 1 for comparability. In addition, in order to indicate the effect of the adaptive learning rate, we set up a comparative experiment with a constant learning rate ($\alpha = 0.01$) in the proposed algorithm, which is called the constant learning rate nonuniformity correction (CLR-NUC). Another three effective NUC algorithms are selected to compare with the proposed algorithm, which are (1) the total variation approach for

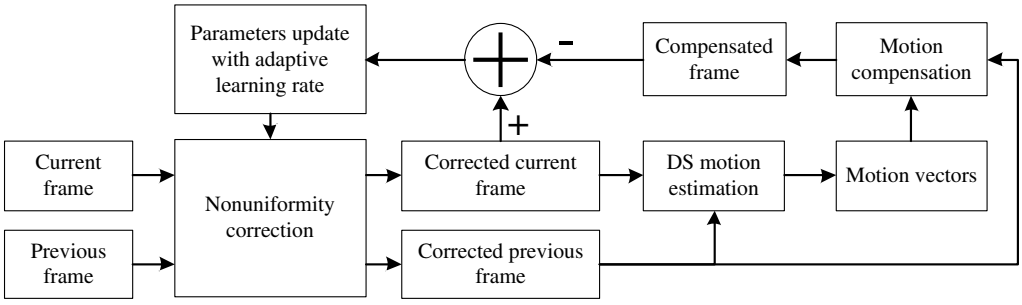

Fig. 4. Flow chart of the proposed NUC algorithm.

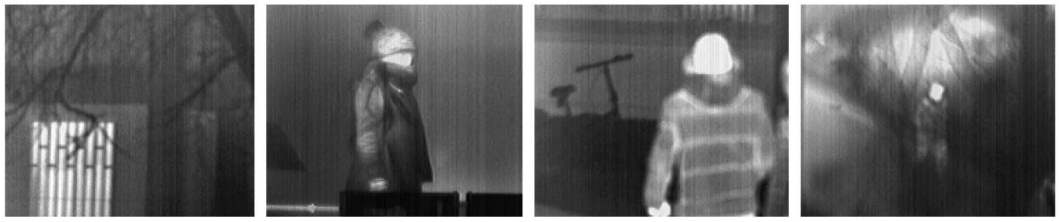

Fig. 5. Original image. (a) Sequence 1, (b) sequence 2, (c) sequence 3, and (d) sequence 4.

adaptive nonuniformity correction (TV-NUC) [12], (2) the bilateral-filter-based temporal high-pass nonuniformity correction (BFTH-NUC) [9], and (3) the interframe-registration-based nonuniformity correction (IRLMS-NUC) [14]. A group of experimental results of these four sequences are shown in Figs. 6–9, respectively.

B. Results and Analysis

The TV-NUC updates the correction parameters based on the anisotropic diffusion effect. Because of the difference of the anisotropic diffusion parameter between the smooth area and the sharp area, ghosting can be suppressed. As can be seen from the correction results, the FPN has been removed partly with little ghosting. However, this is not a useful strategy because it cannot control the correction degree and cannot protect static objects. Thus, in the static place, serious image blurring will occur. As can be seen in Fig. 7(c), the pipeline in the left bottom becomes fuzzy.

As can be seen from the results of BFTH-NUC, there are slight FPNs left. It is always a difficult task to determine the bilateral filter parameter. If more parts of the image are separated to the spatial high frequency, the FPN can be removed totally, but the details of the image will be fuzzy. Otherwise, more FPN would remain. This algorithm cannot distinguish the image details and the FPN adaptively. Besides, omitting the gain part of the FPN is the inherent drawback of THP-NUC. Nevertheless, this algorithm has a comparatively strong practicability.

The IRLMS-NUC adopts the phase-correlation algorithm to calculate the global motion vector. It is not applicable in the situation where both a moving object and a static background scene exist. It achieves good performance in Fig. 6(e), because the scene in this sequence shares the same motion vectors. However, in Figs. 7(e)–9(e), a lot of residual FPN can be seen. Thus, this algorithm is only applicable under the special condition that all objects in the scene share the same motion vectors.

As can be seen from the results of CLR-NUC, Figs. 6(b)–9(b), there are serious locking artifacts. In Fig. 7(b), when the girl turned back, some deformations occur between two adjacent frames, and it is hard for the block matching algorithm to find the optimal points and achieve the correct motion vectors. The incorrect vectors lead to blocking artifact, which impact the correction results seriously. In Fig. 8(b), the rotation of the camera and the shape changes of the objects caused many matching errors, which lead to serious image degradation. Figures 6(b) and 9(b) have comparatively good visual effects, because the motions between the two adjacent frames are simple and matching errors are fewer.

The correction results of the proposed algorithm is indicated in Figs. 6(a)–9(a). Due to the DS block matching algorithm and the adaptive learning rate, the stripe FPN is mostly removed and the phenomenon of ghosting and image blurring does not occur. The purpose of the adaptive learning rate is to eliminate the error of the DS block matching algorithm. The purpose of the DS block matching algorithm is to achieve accurate transform pairs. As can be seen from the correction results, FPN is limited and there is no blocking artifact in the smooth area. No matter how the scene moves and objects change, the proposed algorithm can handle the FPN well.

According to the analysis above, the results of the proposed algorithm have the best visual effects in both sequences.

In addition, the roughness (ρ) [20] is utilized to evaluate the quality of the correction results, defined as

$$\rho = \frac{\|h_1 * x\|_1 + \|h_2 * x\|_1}{\|x\|_1}, \tag{14}$$

Fig. 6. Results of sequence 1 (see Visualization 1). (a) Proposed algorithm, (b) CLR-NUC, (c) TV-NUC, (d) BFTH-NUC, and (e) IRLMS-NUC.

Fig. 7. Results of sequence 2 (see Visualization 2). (a) Proposed algorithm, (b) CLR-NUC, (c) TV-NUC, (d) BFTH-NUC, and (e) IRLMS-NUC.

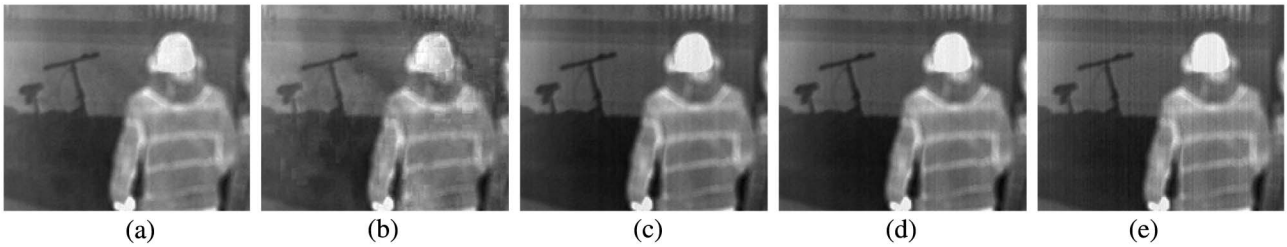

Fig. 8. Results of sequence 3 (see Visualization 3). (a) Proposed algorithm, (b) CLR-NUC, (c) TV-NUC, (d) BFTH-NUC, and (e) IRLMS-NUC.

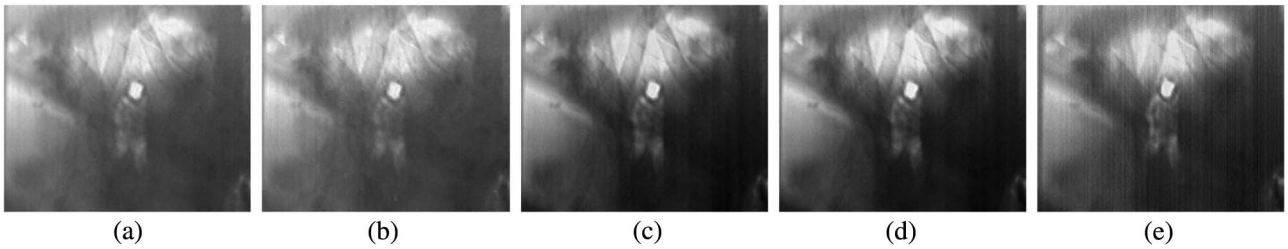

Fig. 9. Results of sequence 4 (see Visualization 4). (a) Proposed algorithm, (b) CLR-NUC, (c) TV-NUC, (d) BFTH-NUC, and (e) IRLMS-NUC.

where x is the infrared image under analysis, $h_1 = [1, -1]$ is a horizontal mask, and $h_2 = h_1^{\mathrm{T}}$ is a vertical mask. The operator $*$ indicates the discrete convolution operation; $\|\|_1$ indicates the L1 norm. Actually, the roughness reflects the degree of variation of the image gradient. A smaller roughness indicates that the correction result is smoother than before. Generally, the smaller the roughness is, the better the correction result will achieve. However, a lower roughness value can also mean that the scene has lost many details during the parameters' estimation. Thus, when the roughness is introduced as an evaluation parameter, the corrected images should also be taken into account and Visualization 1, Visualization 2, Visualization 3, and Visualization 4 should be watched to perform a visual evaluation. The roughness curves of the experimental results are shown in Figs. 10–13, respectively.

As can be seen from the roughness curves of the BFTH-NUC, the convergence rate is remarkable in the first several frames due to the outstanding denoising algorithm, bilateral filter. The convergence rate is much faster than other algorithms. However, as can be seen in Fig. 10, after approximate 100 frames, the advantage is not obvious and the image quality cannot improve any further. The reasons are as follows. First, the bilateral filter cannot completely separate the FPN from the original image. The quality of the desired image is totally dependent on the bilateral filter. Second, this algorithm cannot handle the gain part of the FPN. Thus, FPN cannot be removed totally.

As can be seen from the roughness curves of the TV-NUC, the TV-NUC algorithm has the lowest convergence rate among these NUC algorithms, except the IRLMS-NUC. Although the anisotropic diffusion effect is a useful strategy to suppress ghosting, this algorithm cannot adjust parameters adaptively. The learning rate is fixed, and a large learning rate would lead to unsteady correction results and a small one would lead to lower convergence rates. Thus, it needs more time to converge. For the TV-NUC algorithm, approximately 200 frames are needed to catch up with the BFTH-NUC, as shown in Fig. 10, and the performance of TV-NUC exceeds the BF-NUC after 220 frames, as shown in Fig. 13.

As can be seen in Fig. 10, the IRLMS-NUC algorithm can achieve good performance because the motion in this sequence is simple and one global vector is enough to describe the scene movement. However, the IRLMS-NUC cannot deal with the scene with local motion, as in Figs. 11–13, so roughness is much larger than with the other algorithm.

The CLR-NUC is a simplified version of the proposed algorithm with a constant learning rate, which means that all the pixels in an image share the same learning rate. In the smooth

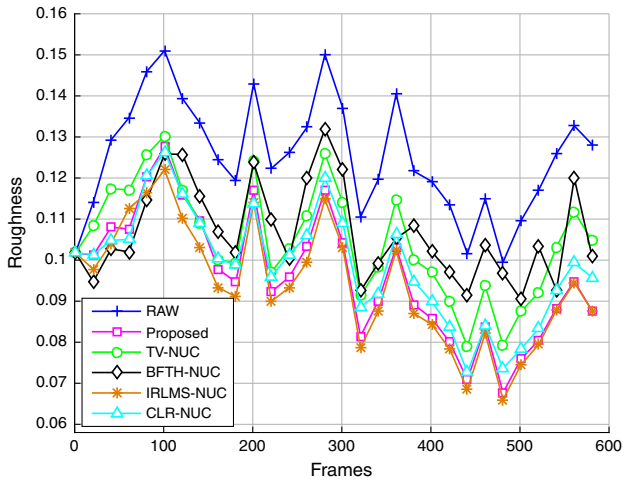

Fig. 10. Roughness of sequence 1.

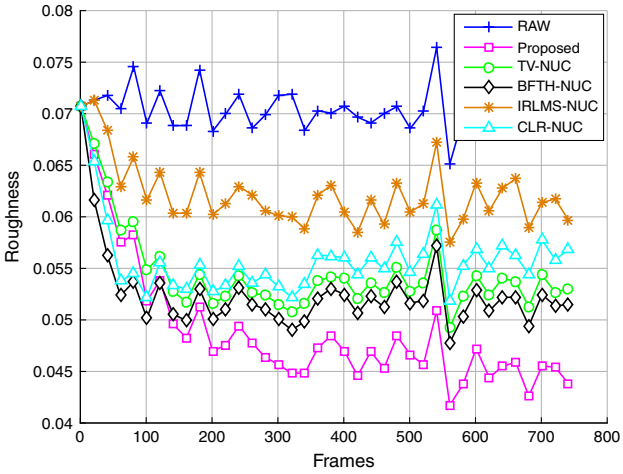

Fig. 11. Roughness of sequence 2.

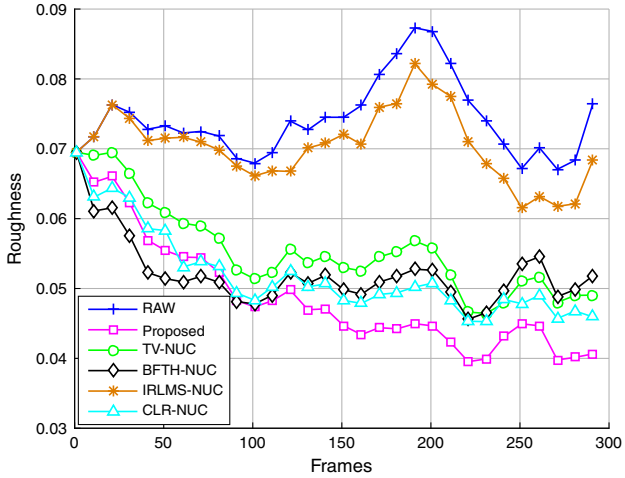

Fig. 13. Roughness of sequence 4.

region, the learning rate may be larger than the adaptive one, and the larger learning rate means a faster convergence rate. Thus, in the first several frames, the roughness is smaller than the proposed algorithm. However, as shown in Fig. 11, with the accumulation of the matching error, the correction performance becomes worse and worse.

For the presented algorithm, accurate transform pairs can be achieved in both simple and complex motion situations due to the DS block matching algorithm. Besides, the adaptive learning rate is also a useful strategy to avoid matching error. However, in Fig. 10, the roughness of the proposed algorithm is larger than IRLMS-NUC in the first 200 frames, because there is not enough movement in some places in the image, especially in the region with the same value. Thus, the correction parameter cannot be updated. In contrast, the IRLMS-NUC only needs one vector to describe motion between two adjacent frames, which is more effective. As the scene changes, all the regions achieve enough motion to update the correction parameters, and then the correction performance of the proposed algorithm can be as good as IRLMS-NUC. Compared with other algorithms, this phenomenon also exists because of the relatively slow initial convergence rate, as shown in Figs. 11–13. In summary, in spite of a slow initial convergence rate, the correction parameter of the proposed algorithm can be steadily updated so that this algorithm can achieve the best performance at last.

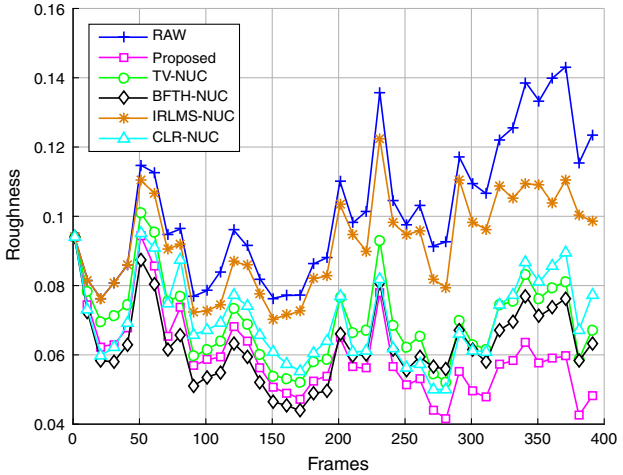

Fig. 12. Roughness of sequence 3.

6. CONCLUSIONS

An improved scene-based nonuniformity correction algorithm for an IRFPA imaging system is proposed. By using an outstanding blocking algorithm and an adaptive learning rate, this algorithm can adapt to complex motion situations with less ghosting and image blurring. However, some places without illumination changes cannot achieve good visual effects in the proposed algorithm. Thus, the correction parameter will not update in these places. Some denoising algorithms may be utilized to process these areas to improve the image quality in the future. Moreover, reducing computational complexity for real-time implementation is another necessary work.

Funding. National Natural Science Foundation of China (NSFC) (61265006, 61401343); Fundamental Research Funds for the Central Universities of China (JDYB140105, JDZD140202, WRYB142312); 863 Program of China (2014AA8098089C).

Acknowledgment. We express our sincere appreciation to the anonymous reviewers for their insightful and valuable comments, which have greatly helped us in improving the quality of the paper.

REFERENCES

1. D. R. Pipa, E. A. B. da Silva, C. L. Pagliari, and P. S. R. Diniz, "Recursive algorithms for bias and gain nonuniformity correction in infrared videos," IEEE Trans. Image Process. **21**, 4758–4769 (2012).
2. A. Friedenberg and I. Goldblatt, "Nonuniformity two-point linear correction errors in infrared focal plane arrays," Opt. Eng. **37**, 1251–1253 (1998).
3. Y. P. Cao and C. L. Tisse, "Shutterless solution for simultaneous focal plane array temperature estimation and nonuniformity correction in

uncooled long-wave infrared camera," Appl. Opt. **52**, 6266–6271 (2013).
4. J. G. Harris and Y. M. Chiang, "Nonuniformity correction of infrared image sequences using the constant-statistics constraint," IEEE Trans. Image Process. **8**, 1148–1151 (1999).
5. D. A. Scribner, K. A. Sarkady, J. T. Caulfield, M. R. Kruer, G. Katz, C. J. Gridley, and C. Herman, "Nonuniformity correction for staring IR focal plane arrays using scene-based techniques," Proc. SPIE **1308**, 224–233 (1990).
6. D. A. Scribner, K. A. Sarkady, M. R. Kruer, J. T. Caulfield, J. D. Hunt, and C. Herman, "Adaptive nonuniformity correction for IR focal-plane arrays using neural networks," Proc. SPIE **1541**, 100–109 (1991).
7. R. C. Hardie, M. M. Hayat, E. Armstrong, and B. Yasuda, "Scene-based nonuniformity correction with video sequences and registration," Appl. Opt. **39**, 1241–1250 (2000).
8. R. C. Hardie, F. Baxley, B. Brys, and P. Hytla, "Scene-based nonuniformity correction with reduced ghosting using a gated LMS algorithm," Opt. Express **17**, 14918–14933 (2009).
9. C. Zuo, Q. A. Chen, G. H. Gu, and W. X. Qian, "New temporal high-pass filter nonuniformity correction based on bilateral filter," Opt. Rev. **18**, 197–202 (2011).
10. J. Q. Bai, H. Y. Hou, C. G. Zhao, N. Sun, and X. Y. Wang, "Adaptive nonuniformity correction for IRFPA sensors based on neural network framework," J. Syst. Eng. Electron **23**, 618–624 (2012).
11. A. Rossi, M. Diani, and G. Corsini, "Bilateral filter-based adaptive nonuniformity correction for infrared focal-plane array systems," Opt. Eng. **49**, 057003 (2010).
12. E. Vera, P. Meza, and S. Torres, "Total variation approach for adaptive nonuniformity correction in focal-plane arrays," Opt. Lett. **36**, 172–174 (2011).
13. E. Vera and S. Torres, "Fast adaptive nonuniformity correction for infrared focal-plane array detectors," EURASIP J. Adv. Signal Process. **2005**, 1994–2004 (2005).
14. C. Zuo, Q. Chen, G. H. Gu, and X. B. Sui, "Scene-based nonuniformity correction algorithm based on interframe registration," J. Opt. Soc. Am. A **28**, 1164–1176 (2011).
15. B. M. Ratliff, M. M. Hayat, and R. C. Hardie, "An algebraic algorithm for nonuniformity correction in focal-plane arrays," J. Opt. Soc. Am. A **19**, 1737–1747 (2002).
16. N. Liu and H. Qiu, "A time-domain projection-based registration-scene-based nonuniformity correction technology and its detailed hardware realization," Opt. Rev. **21**, 17–26 (2014).
17. S. Zhu and K. K. Ma, "A new diamond search algorithm for fast block-matching motion estimation," IEEE Trans. Image Process. **9**, 525 (2000).
18. A. Barjatya, "Block matching algorithms for motion estimation," IEEE Trans. Evol. Comput. **8**, 225–239 (2004).
19. G. A. Triantafyllidis, D. Tzovaras, and M. G. Strintzis, "Blocking artifact detection and reduction in compressed data," IEEE Trans. Circuits Syst. Video Technol. **12**, 877–890 (2002).
20. P. Meza, G. Machuca, S. Torres, C. S. Martin, and E. Vera, "Simultaneous digital super-resolution and nonuniformity correction for infrared imaging systems," Appl. Opt. **54**, 6508–6515 (2015).